

# High-energy neutrino emission from the Type IIn supernova SN 2017hcd

Shunhao Ji<sup>1,\*</sup>, Zhongxiang Wang<sup>1,\*</sup>, Litao Zhu<sup>1</sup> & Dong Zheng<sup>1</sup>

<sup>1</sup>*Department of Astronomy, School of Physics and Astronomy, Key Laboratory of Astroparticle Physics of Yunnan Province, Yunnan University, Kunming 650091, China*

Neutrino astronomy provides another window to exploring the Universe, exemplified by the detection of a megaelectronvolt neutrino burst from the core-collapse supernova (CCSN) SN 1987A (refs. 1,2). Commonly discussed theories suggest that some CCSNe could produce neutrinos with energies a thousand times more than those of SN 1987A <sup>3</sup>, which has been probed with new-generation facilities <sup>4-6</sup>. The interaction of SN ejecta with a dense circumstellar medium (CSM) or a jet, launched in a CCSN, being choked in the stellar envelope of the progenitor or an outside CSM are both well-accepted scenarios for the high-energy neutrino production. Here we report the detection of a high-energy neutrino flare at a  $3.9\sigma$  significance from SN 2017hcd, made by our analysis of the public track-like neutrino data taken by the IceCube Neutrino Observatory <sup>7</sup>. A Type IIn SN with optical emissions arising from the ejecta–CSM interaction, SN 2017hcd’s neutrino flare lasted  $\sim 1-2$  month, with its central time  $\sim 14$ -day prior to the SN’s optical discovery time. Its estimated isotropic neutrino energy (all flavors) is approximately two orders of magnitude higher than the energy ( $\sim 10^{50}$  erg) carried in the SN’s ejecta, too high to be explained with the ejecta–CSM scenario. Thus, a choked jet may be the source of the neutrino flare.

It has been nearly 40 years since the nearby supernova (SN) explosion SN 1987A, which occurred in the Large Magellanic Cloud and whose burst of megaelectronvolt (MeV) neutrinos were successfully detected <sup>1,2</sup>. While new-generation neutrino detectors are eagerly waiting to detect such events from similar core-collapse SNe (CCSNe) that are expected to occur once every

$\sim 30$  years in the Milky Way <sup>8</sup>, the IceCube neutrino observatory <sup>7</sup> at the South Pole, as well as several other detectors, have opened a multi-messenger window for detecting gigaelectronvolt (GeV) to teraelectronvolt (TeV) neutrinos emitted from astrophysical objects <sup>9–12</sup>, and have since been used to search for high-energy neutrinos emitted from CCSNe <sup>4–6,13–16</sup>.

The CCSNe, which mark the deaths of massive stars, are among the most luminous transient phenomena in the Universe. In addition to the burst of MeV neutrinos produced in their core-collapse process <sup>8</sup>, it has been widely discussed that when there is a substantially dense circumstellar medium (CSM) around a CCSN, which is present due to the progenitor’s significant mass loss in the years before the explosion <sup>17,18</sup>, high-energy GeV–TeV neutrinos would also be produced through the interaction of the SN’s ejecta with the CSM <sup>3</sup>. As a subclass of Type II SNe, the Type IIn SNe (SNe IIn) are characterized by optical spectra with narrow Balmer emission lines, an indication of shock interaction between the SN ejecta and the CSM. SNe IIn are thus considered as particularly promising targets for detecting high-energy neutrinos from CCSNe.

SN 2017hcd was discovered by the Asteroid Terrestrial-impact Last Alert System (ATLAS) <sup>19</sup> on October 1 2017 (MJD 58027.48) at the position of R.A. =  $25^{\circ}.71604$ , Decl. =  $+31^{\circ}.48238$  (J2000). It was classified as an SN IIn with a redshift  $z$  of 0.035 (see section ‘Photometric data and light-curve analysis’), which corresponds to a luminosity distance of 159.2 megaparsec (Mpc). It is located at the edge of the nearby galaxy MCG+05-05-002 (see Extended Data Fig. 1) and should be associated with this galaxy given that they both have the same redshift value. The optical light curves of SN 2017hcd (Fig. 1 and Extended Data Fig. 2), although only mainly at ATLAS  $o$  band, are generally similar to those of SNe IIn <sup>20,21</sup>, and we estimated a total radiation energy of  $\sim 10^{50}$  erg from analyzing the light curves (see section ‘Photometric data and light-curve analysis’). An optical spectrum of SN 2017hcd was taken 16 days after the discovery, and it also shows features typical of SNe IIn (Extended Data Fig. 3; see section ‘Optical spectrum analysis’).

We searched for neutrino emissions from SN 2017hcd by performing a time-dependent un-

binned maximum likelihood analysis to the public data provided by IceCube, which are implemented in the `SKYLLH` framework released by IceCube (see section ‘IceCube data analysis’). An *a priori* time window  $T_{\text{win}}$  for the search was set to be 300 days, from MJD 57950 to MJD 58250 (Fig. 1). This window was such that not only was the property of SNe IIn considered, whose shock breakout (SBO) occurs in the CSM and whose explosion is several tens of days before the SBO<sup>20</sup>, but it also fully covered SN 2017hcd’s optical flare as well. Within  $T_{\text{win}}$ , neutrino events were expected to cluster in time, and we set two time profiles: a Gauss and a box. The neutrino flux  $\Phi_{\nu_\mu+\bar{\nu}_\mu}$  was assumed to have a power-law energy spectrum with index  $\gamma$ ,  $\Phi_{\nu_\mu+\bar{\nu}_\mu} = \Phi_0(E_{\nu_\mu}/E_0)^{-\gamma}$ , where  $E_{\nu_\mu}$  is neutrino energy,  $E_0$  is fixed at 1 TeV, and  $\Phi_0$  is the flux normalization.

From the search analysis, we found a significant neutrino flare at SN 2017hcd’s position with both time profiles (Table 1 and Fig. 1). The box profile resulted in a higher significance value,  $3.9\sigma$ , estimated from the obtained test statistic (TS) value of 26.3 after considering a trial factor of 2 (ref. 10; see section ‘IceCube data analysis’). The flare, with the determined central time  $T_0$  at  $\sim$ MJD 58013, preceded the optical emission of the SN by  $\sim$ 10 days and had a time duration  $T_W$  of approximately 34 (from the Gaussian profile) to 54 days (from the box profile). The flare consisted of an event excess  $n_s$  of 7–17 muon neutrinos in addition to the atmospheric and diffuse cosmic background neutrinos. We also calculated the weights of the long-term events at the position of the SN, and an event clustering at the SN’s explosion time is clearly observed (Fig. 2). We further obtained a TS map during the neutrino flare period (i.e.,  $T_W$  from the box time profile) by scanning a  $4^\circ \times 4^\circ$  sky region centered at SN 2017hcd (Fig. 3), and SN 2017hcd was only  $\sim 0.18^\circ$  away from the hottest location of the neutrino emission.

The detection of a high-energy neutrino flare from an SN IIn matches the theoretical expectations<sup>22–24</sup>. A shock arising from the collision of the SN ejecta with a CSM accelerates cosmic rays (CRs), which collide with the CSM nucleons ( $pp$  interaction), leading to the production of neutrinos and high-energy  $\gamma$ -rays. It is particularly notable that the neutrino flare started at the estimated explosion time of SN 2017hcd and approximately ended after the shock breakout in the CSM

(Fig. 1; see ‘Photometric data and light-curve analysis’). We searched for  $\gamma$ -ray emissions from the SN by analyzing the data obtained with the Large Area Telescope (LAT) onboard *the Fermi Gamma-ray Space Telescope*. No emissions were detected (resulting in an upper limit on the flux in 0.1–500 GeV,  $\leq 8.4 \times 10^{-12} \text{ erg cm}^{-2} \text{ s}^{-1}$ ; see section ‘*Fermi*-LAT data analysis’). The non-detection could be due to attenuation on matter and radiation in the CSM<sup>22,25,26</sup>. However, the estimated isotropic neutrino luminosity at 1 TeV (from the box profile) was  $L_{\nu,\text{iso}} \simeq 3.6 \times 10^{45} \text{ erg s}^{-1}$  and the all-flavor isotropic neutrino energy at 1 TeV was  $E_{\nu,\text{iso}} \simeq L_{\nu,\text{iso}} T_W / (1+z) \approx 1.7 \times 10^{52} \text{ erg}$ , too high to be explained by the ejecta–CSM interaction scenario, as the total radiation energy estimated from the optical light curves was only  $\sim 10^{50} \text{ erg}$  (see section ‘Photometric data and light-curve analysis’). The latter is considered to indicate the order-of-magnitude value for the SN’s kinetic energy,  $\sim 10\%$  of which would go into CRs’ energy<sup>22,24,25</sup>. The energy mismatch has been reflected in theoretical studies that only CCSNe (including SNe IIn) within 10 Mpc are shown to have potentially detectable neutrino emissions<sup>24,27,28</sup>.

Another widely discussed scenario for the cause of high-energy neutrino emissions from CCSNe are choked jets<sup>29,30</sup>, which are considered to be launched in the same manner as those of gamma-ray bursts (GRBs), only slower than the latter. They can not break through either the envelope of a progenitor star or a pre-existing dense CSM<sup>31,32</sup>. The shock in such a jet accelerates protons, which interact with photons ( $p\gamma$  interaction) and/or protons, producing high-energy neutrinos<sup>33,34</sup>. The relativistic beaming of this jet can significantly boost the observed neutrino flux<sup>4,13</sup>, similar to the mechanism through which emissions are boosted in GRBs; the inferred isotropic radiation energies of GRBs are typically as high as  $\sim 10^{52} \text{ erg}$ <sup>35</sup>. Thus, the neutrino flare of SN 2017hcd might arise from a choked jet, and the beaming effect of the jet helped enable the detection. The flare’s duration may indicate that the ‘unseen’ jet had a  $\sim 1$ – $2$  month lifespan. Such a long-lived jet is possible if it is powered by the accretion of the progenitor’s mass onto a newly formed black hole in an SN<sup>32,36</sup>. The neutrino emission in this SN case was soft ( $\gamma \sim 3.5$ ),

comparable to that detected from the nearby active galaxy NGC 1068<sup>11</sup>. Such soft emissions have been discussed to reflect the strong cooling effects in the emission region<sup>4,33</sup>. Analogous to the role of NGC 1068 (ref. 37), this SN case likely shows that ‘hidden’ jets of CCSNe are another type of high-energy neutrino source in the Universe.

## References

1. Hirata, K. *et al.* Observation of a neutrino burst from the supernova SN1987A. *Phys. Rev. Lett.* **58**, 1490–1493 (1987).
2. Bionta, R. M. *et al.* Observation of a neutrino burst in coincidence with supernova 1987A in the Large Magellanic Cloud. *Phys. Rev. Lett.* **58**, 1494–1496 (1987).
3. Tamborra, I. & Murase, K. Neutrinos from Supernovae. *Space. Sci. Reviews.* **214**, 31 (2018).
4. Abbasi, R. *et al.* Searching for soft relativistic jets in core-collapse supernovae with the IceCube optical follow-up program. *Astron. Astrophys.* **539**, A60 (2012). 1111.7030.
5. Aartsen, M. G. *et al.* The Detection of a Type II<sub>n</sub> Supernova in Optical Follow-up Observations of IceCube Neutrino Events. *Astrophys. J.* **811**, 52 (2015). 1506.03115.
6. Abbasi, R. *et al.* Constraining High-energy Neutrino Emission from Supernovae with IceCube. *Astrophys. J. Let.* **949**, L12 (2023). 2303.03316.
7. Aartsen, M. G. *et al.* The IceCube Neutrino Observatory: instrumentation and online systems. *Journal of Instrumentation* **12**, P03012 (2017). 1612.05093.
8. Horiuchi, S. & Kneller, J. P. What can be learned from a future supernova neutrino detection? *Journal of Physics G Nuclear Physics* **45**, 043002 (2018). 1709.01515.
9. IceCube Collaboration *et al.* Multimessenger observations of a flaring blazar coincident with high-energy neutrino IceCube-170922A. *Science* **361**, eaat1378 (2018). 1807.08816.

10. IceCube Collaboration *et al.* Neutrino emission from the direction of the blazar TXS 0506+056 prior to the IceCube-170922A alert. *Science* **361**, 147–151 (2018). 1807.08794.
11. IceCube Collaboration *et al.* Evidence for neutrino emission from the nearby active galaxy NGC 1068. *Science* **378**, 538–543 (2022). 2211.09972.
12. Icecube Collaboration *et al.* Observation of high-energy neutrinos from the Galactic plane. *Science* **380**, 1338–1343 (2023). 2307.04427.
13. IceCube Collaboration *et al.* Constraints on high-energy neutrino emission from SN 2008D. *Astron. Astrophys.* **527**, A28 (2011). 1101.3942.
14. Senno, N., Murase, K. & Mészáros, P. Constraining high-energy neutrino emission from choked jets in stripped-envelope supernovae. *Journal of Cosmology and Astroparticle Physics* **2018**, 025 (2018). 1706.02175.
15. Chang, P.-W., Zhou, B., Murase, K. & Kamionkowski, M. High-energy neutrinos from choked-jet supernovae: Searches and implications. *Phys. Rev. D* **109**, 103041 (2024). 2210.03088.
16. Stein, R. *et al.* SN 2023uqf: An Interacting Supernova Coincident with a High-Energy Neutrino. *arXiv e-prints* arXiv:2508.08355 (2025). 2508.08355.
17. Ofek, E. O. *et al.* Precursors Prior to Type II<sub>n</sub> Supernova Explosions are Common: Precursor Rates, Properties, and Correlations. *Astrophys. J.* **789**, 104 (2014). 1401.5468.
18. Ransome, C. L. *et al.* A systematic reclassification of Type II<sub>n</sub> supernovae. *Mon. Not. R. Astron. Soc.* **506**, 4715–4734 (2021). 2107.02179.
19. Tonry, J. L. *et al.* ATLAS: A High-cadence All-sky Survey System. *Publ. Astron. Soc. Pac.* **130**, 064505 (2018). 1802.00879.

20. Moriya, T. J. *et al.* Mass-loss histories of Type II<sub>n</sub> supernova progenitors within decades before their explosion. *Mon. Not. R. Astron. Soc.* **439**, 2917–2926 (2014). 1401.4893.
21. Ransome, C. L. & Villar, V. A. Unveiling the Diversity of Type II<sub>n</sub> Supernovae via Systematic Light-curve Modeling. *Astrophys. J.* **987**, 13 (2025). 2409.10596.
22. Murase, K., Thompson, T. A., Lacki, B. C. & Beacom, J. F. New class of high-energy transients from crashes of supernova ejecta with massive circumstellar material shells. *Phys. Rev. D* **84**, 043003 (2011). 1012.2834.
23. Katz, B., Sapir, N. & Waxman, E. X-rays,  $\gamma$ -rays and neutrinos from collisionless shocks in supernova wind breakouts. In Roming, P., Kawai, N. & Pian, E. (eds.) *Death of Massive Stars: Supernovae and Gamma-Ray Bursts*, vol. 279 of *IAU Symposium*, 274–281 (2012). 1106.1898.
24. Murase, K. New prospects for detecting high-energy neutrinos from nearby supernovae. *Phys. Rev. D* **97**, 081301 (2018). 1705.04750.
25. Margutti, R. *et al.* A Panchromatic View of the Restless SN 2009ip Reveals the Explosive Ejection of a Massive Star Envelope. *Astrophys. J.* **780**, 21 (2014). 1306.0038.
26. Ackermann, M. *et al.* Search for Early Gamma-ray Production in Supernovae Located in a Dense Circumstellar Medium with the Fermi LAT. *Astrophys. J.* **807**, 169 (2015). 1506.01647.
27. Kheirandish, A. & Murase, K. Detecting High-energy Neutrino Minibursts from Local Supernovae with Multiple Neutrino Observatories. *Astrophys. J. Let.* **956**, L8 (2023). 2204.08518.
28. Valtonen-Mattila, N. & O’Sullivan, E. Prospects for Extending the Core-collapse Supernova Detection Horizon Using High-energy Neutrinos. *Astrophys. J.* **945**, 98 (2023). 2206.00450.

29. Mészáros, P. & Waxman, E. TeV Neutrinos from Successful and Choked Gamma-Ray Bursts. *Phys. Rev. Lett.* **87**, 171102 (2001). astro-ph/0103275.
30. Razzaque, S., Mészáros, P. & Waxman, E. TeV Neutrinos from Core Collapse Supernovae and Hypernovae. *Phys. Rev. Lett.* **93**, 181101 (2004). astro-ph/0407064.
31. Nakar, E. A Unified Picture for Low-luminosity and Long Gamma-Ray Bursts Based on the Extended Progenitor of IIGRB 060218/SN 2006aj. *Astrophys. J.* **807**, 172 (2015). 1503.00441.
32. He, H.-N., Kusenko, A., Nagataki, S., Fan, Y.-Z. & Wei, D.-M. Neutrinos from Choked Jets Accompanied by Type-II Supernovae. *Astrophys. J.* **856**, 119 (2018). 1803.07478.
33. Ando, S. & Beacom, J. F. Revealing the Supernova Gamma-Ray Burst Connection with TeV Neutrinos. *Phys. Rev. Lett.* **95**, 061103 (2005). astro-ph/0502521.
34. Murase, K. & Ioka, K. TeV-PeV Neutrinos from Low-Power Gamma-Ray Burst Jets inside Stars. *Phys. Rev. Lett.* **111**, 121102 (2013). 1306.2274.
35. Tsvetkova, A. *et al.* The Konus-Wind Catalog of Gamma-Ray Bursts with Known Redshifts. II. Waiting-Mode Bursts Simultaneously Detected by Swift/BAT. *Astrophys. J.* **908**, 83 (2021). 2012.14849.
36. Liu, T., Song, C.-Y., Yi, T., Gu, W.-M. & Wang, X.-F. A possible feedback mechanism of outflows from a black hole hyperaccretion disk in the center of jet-driven iPTF14hls. *Journal of High Energy Astrophysics* **22**, 5–9 (2019). 1902.03464.
37. Murase, K., Kimura, S. S. & Mészáros, P. Hidden Cores of Active Galactic Nuclei as the Origin of Medium-Energy Neutrinos: Critical Tests with the MeV Gamma-Ray Connection. *Phys. Rev. Lett.* **125**, 011101 (2020). 1904.04226.

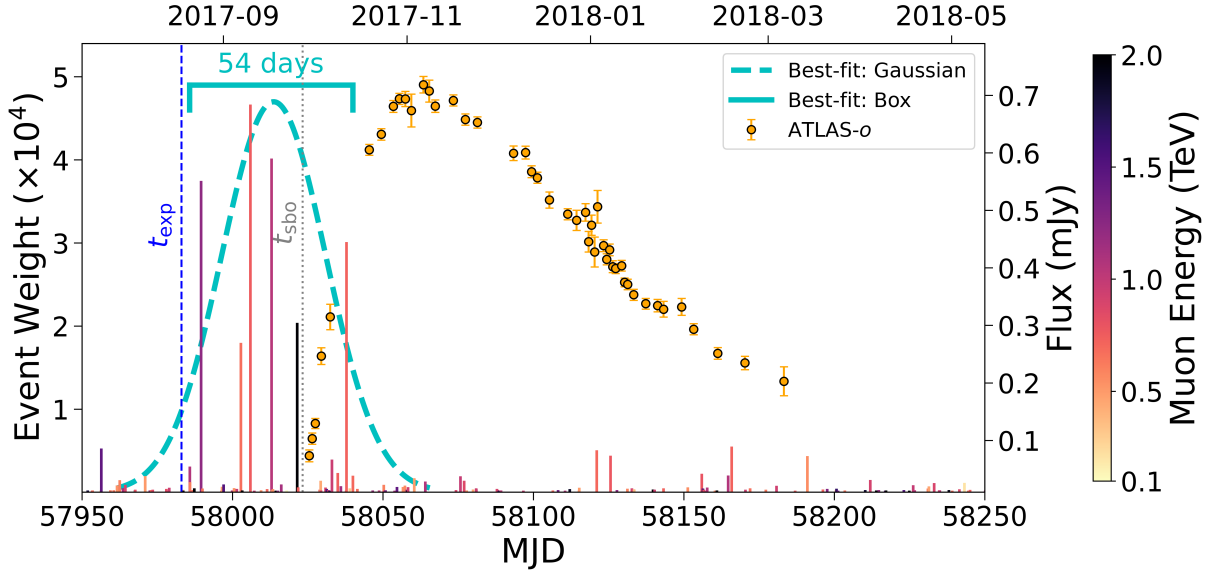


Figure 1: **Neutrino flare determined at SN 2017hcd's position.** The colored vertical lines are the individual neutrino events detected, with their heights being the weights (calculated with  $\gamma = 3.5$ ; see section ‘IceCube data analysis’) and their colors being the reconstructed muon energies (indicated by the right-side color bar). The time durations of the flare, from the box and Gaussian time profile (marked by the 54-days cyan line and cyan dashed curve respectively) are shown. The whole X-axis time duration is the *a priori* window  $T_{\text{win}}$ , within which the flare was searched. The central times of the durations precede the shock breakout time (marked by the gray dotted line) of the SN by  $\sim 10$  days; the latter was determined from the ATLAS o-band light curve (orange dots; see section ‘Photometric data and light-curve analysis’). The estimated explosion time of the SN is marked by a blue dashed line.

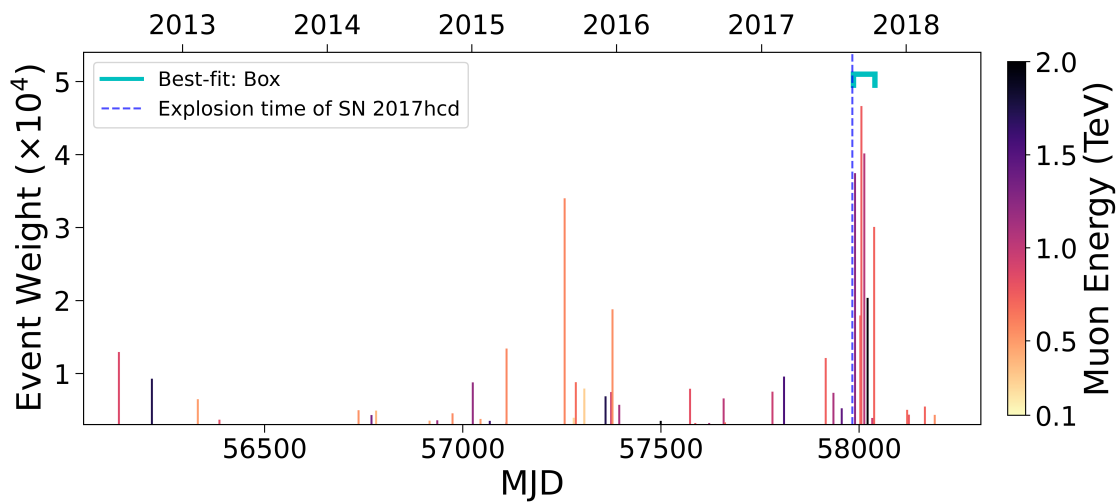


Figure 2: **Neutrino events detected at SN 2017hcd’s position during the IceCube season IC86-II–VII.** The weights and reconstructed muon energies of the events, the SN’s estimated explosion time, and the neutrino flare’s duration from the box time profile are respectively indicated as the same as those in Fig. 1. A clustering of high-weighted events at the SN explosion time is clearly visible.

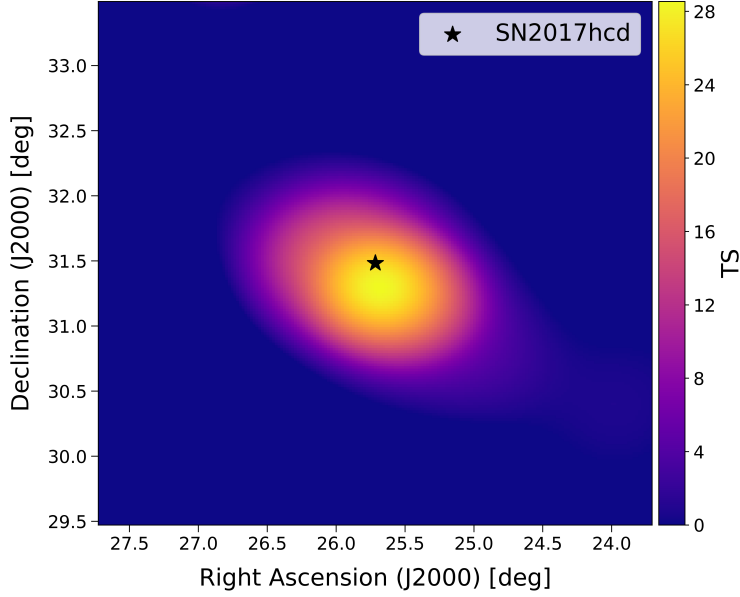


Figure 3: **Neutrino TS map of a  $4^\circ \times 4^\circ$  region around SN 2017hcd (whose position is marked by a black star) during the best-fit flare period.** The map was calculated using the box time profile, and the spectral index and time PDF were fixed at the best-fit values (see section ‘IceCube data analysis’).

Profile	$T_0$ (MJD)	$T_W$ (MJD)	$\gamma$	$n_s$	$\Phi_{\nu_\mu + \bar{\nu}_\mu}^{1\text{TeV}} / 10^{-10}$ ( $\text{TeV}^{-1} \text{cm}^{-2} \text{s}^{-1}$ )	TS	Significance
Gauss	$58014_{-7}^{+9}$	$34_{-6}^{+30}$	$3.5_{-0.6}^{+0.5}$	$11_{-4}^{+5}$	$3.5_{-1.2}^{+1.5}$	20.2	$3.9\sigma$
Box	58012.9	54.3	$3.5_{-0.6}^{+0.5}$	$13_{-4}^{+4}$	$2.5_{-0.8}^{+0.9}$	26.3	$4.0\sigma$

Table 1: **Neutrino analysis results for two time profiles.** Columns  $T_0$  and  $T_W$  are the central time and duration of the flare, respectively; for the Gaussian time profile,  $T_W$  is given as  $2\sigma_T$  (section ‘IceCube data analysis’). Columns  $n_s$  and  $\Phi_{\nu_\mu + \bar{\nu}_\mu}^{1\text{TeV}}$  are the net neutrino number and the flux normalization at 1 TeV over  $T_W$ , respectively. Uncertainties are at a 68% confidence level, but the upper bound values on  $\gamma$  are limited by the setting of  $\gamma \leq 4.0$  in our neutrino data analysis.

## Methods

### 1 Photometric data and light-curve analysis

**Photometric data** The discovery of SN 2017hcd was made by ATLAS on October 1 2017 at its *o* band <sup>38</sup>, which was reported in the Transient Name Server (TNS)<sup>1</sup>. It was classified as an SN II<sub>n</sub> with redshift  $z = 0.035$  (ref. 39). Its position was at the edge of a nearby galaxy MCG+05-05-002, which has the same redshift value <sup>40</sup> and therefore is likely the host galaxy (Extended Data Fig. 1). Its distance to the center of the galaxy is  $\sim 15''$ , which corresponds to  $\approx 11.6$  kpc at a source distance of 159.2 Mpc.

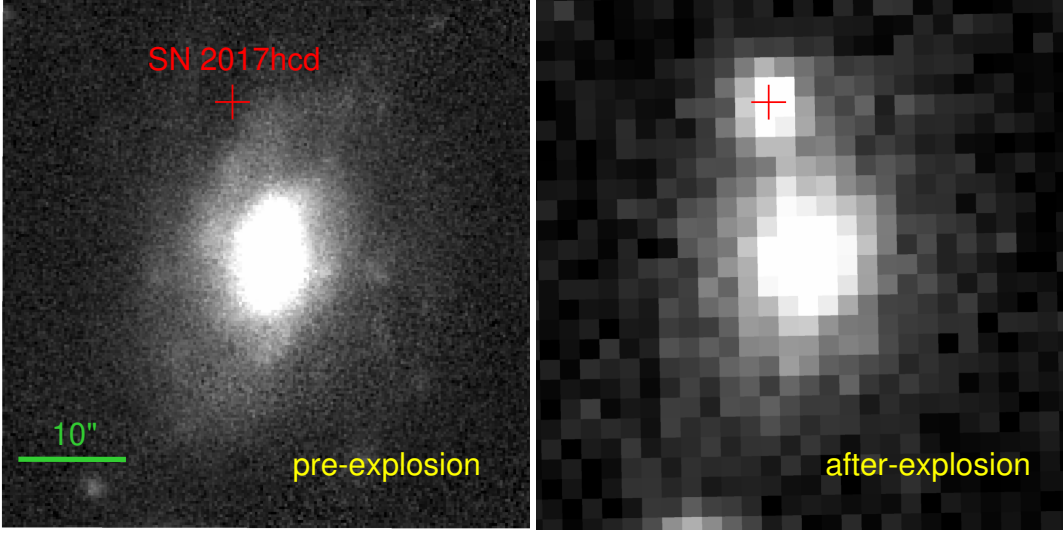
The ATLAS *o*-band data provide a good coverage of the entire explosion (see Fig. 1). Additionally, there were a few measurements at ATLAS *c* band, Gaia *G* band (from the Gaia Photometric Science Alerts <sup>2</sup>), Pan-STARRS *i* band, and Sloan *g* band. The ATLAS data were from the ATLAS forced photometry server <sup>41</sup>, and were cleaned and binned for each night by using ATClean <sup>42</sup>; we excluded any data points with flux errors  $> 0.1$  mJy. The non-ATLAS measurements were given on TNS. For the Gaia *G*-band data, the median standard deviations of different Gaia-*G* magnitudes given in ref. 43 were taken as the uncertainties. For the single Sloan *g*-band data point, we assigned 0.1 mag as its error because no uncertainty was reported.

**ATLAS *o*-band light curve fitting** When an SN explodes in a dense CSM, which is sufficiently opaque to radiation, the shock breakout (SBO) will occur in the CSM rather than the stellar surface <sup>45</sup>. For a CSM with a wind extent of radius  $R_w$ , larger than the radiation diffusion radius  $R_d$ , the SBO time  $t_{\text{sbo}}$  occurs at  $\sim t_d = R_d/v_{\text{sh}}$ , where  $v_{\text{sh}}$  is the shock velocity, and the light-curve rising time  $t_{\text{rise}}$  from the SBO to the peak is also  $\sim t_d$  (ref. 45). The occasional flattening seen in the declining phase of the light curve of SN 2017hcd suggests that this SN case had  $R_w > R_d$  (ref. 45). In order to estimate the light-curve peak time,  $t_{\text{peak}}$ , and  $t_{\text{rise}}$ , we used a parabolic function

---

<sup>1</sup><https://www.wis-tns.org/object/2017hcd>

<sup>2</sup><https://gsaweb.ast.cam.ac.uk/alerts/alert/Gaia17dgr/>



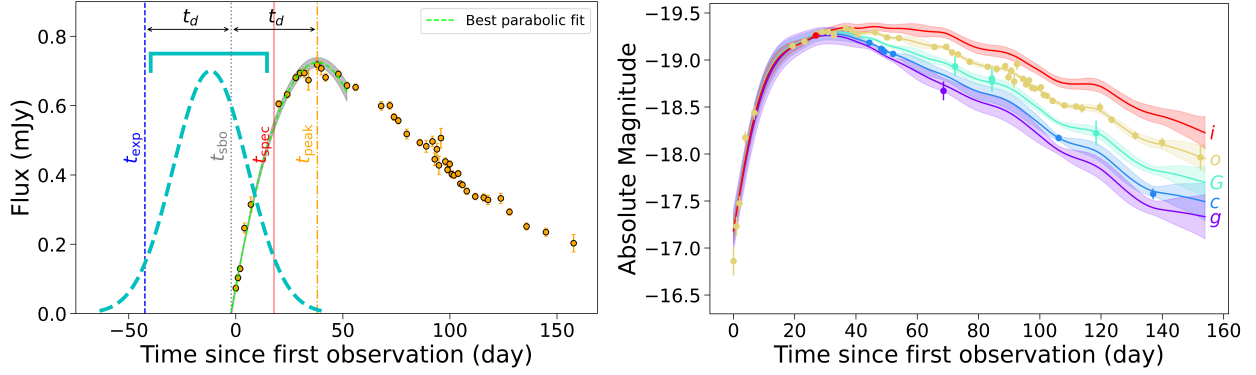
Extended Data Fig. 1: **Optical images centered at the host galaxy of SN 2017hcd, MCG+05-05-002.** *Left panel:* Pan-STARRS *i*-band image <sup>44</sup> taken before the explosion of SN 2017hcd. *Right panel:* ATLAS *o*-band image taken at  $\sim 54$  days after the discovery time. In both panels, the red cross indicates the location of SN 2017hcd.

<sup>46</sup>,

$$F(t) = F_{\text{peak}} \left[ 1 - \left( \frac{t - t_{\text{peak}}}{t_{\text{rise}}} \right)^2 \right], \quad (1)$$

where the flux density  $F(t)$  reaches the peak  $F_{\text{peak}}$  at time  $t_{\text{peak}}$ , and  $t_{\text{rise}}$  is the duration from zero to  $F_{\text{peak}}$ . To fit the rise of the ATLAS *o*-band light curve with this function, we applied the Markov Chain Monte Carlo (MCMC) method, implemented by Python package `emcee` <sup>47</sup>. From the fitting, we obtained  $t_{\text{rise}} = 40_{-1}^{+2}$  day with  $t_{\text{peak}}$  at MJD  $58063_{-1}^{+2}$  ( $F_{\text{peak}} = 0.72 \pm 0.01$  mJy). As the fit gave  $t_{\text{sbo}} \sim \text{MJD } 58023$  when the flux was zero and  $t_d \sim t_{\text{rise}} \simeq 40$  day, the SN explosion time  $t_{\text{exp}}$  was estimated to be  $\sim 40$  day before the SBO, at  $\sim \text{MJD } 57983$ . The estimated  $t_{\text{exp}}$  is remarkably close to the onset time of the neutrino flare set by the box time profile, which is at  $\sim \text{MJD } 57986$  (Extended Data Fig 2).

**Radiation energy estimate** Multi-band ultraviolet, optical, and infrared light curves of SNe IIn are often used to construct their bolometric light curves, which provide estimates for their total radi-



Extended Data Fig. 2: **Left:** parabolic fit (green dashed curve) to the ATLAS *o*-band light curve and the estimated shock-breakout time (marked by the gray dotted line) in the CSM. The orange dash-dotted line indicates the flux peak time of the light curve, and the blue dashed line indicates the estimated explosion time of SN 2017hcd. The observation time of the spectrum (shown in Extended Data Fig. 3) is marked by the red line. The determined two neutrino-flare time profiles (Fig. 1) are also shown for comparison. **Right:** *extrabol* fits to the multi-band data points of SN 2017hcd. The bands of the data points are marked at the right side of the fits.

ation energy. However, we did not find other data except those reported on TNS mentioned above. In addition, the multi-band light curves can be used to construct spectral energy distributions at different epochs, which can be fitted with a blackbody (BB) function (e.g., ref. 48). In order to estimate the radiation energy from SN 2017hcd, we used a python-based package *extrabol*<sup>49</sup> to estimate its bolometric light curve. This package uses Gaussian Process regression for light curve estimation and then fits the light curves with BB functions to obtain the bolometric light curve. By performing the fitting to the multi-band data (Extended Data Fig. 2), in which we adopted the Galactic reddening  $E(B - V) = 0.0524$ <sup>50</sup>, we obtained  $\sim 1 \times 10^{50}$  erg for the total radiation energy from the trapezoidal integral of the estimated bolometric light curve. In the fitting, the temperature and radius of the BB functions were in ranges of 5000–9000 K and  $(1-3) \times 10^{15}$  cm, respectively. The ranges are consistent with those reported for other SNe IIn (e.g., ref. 48).

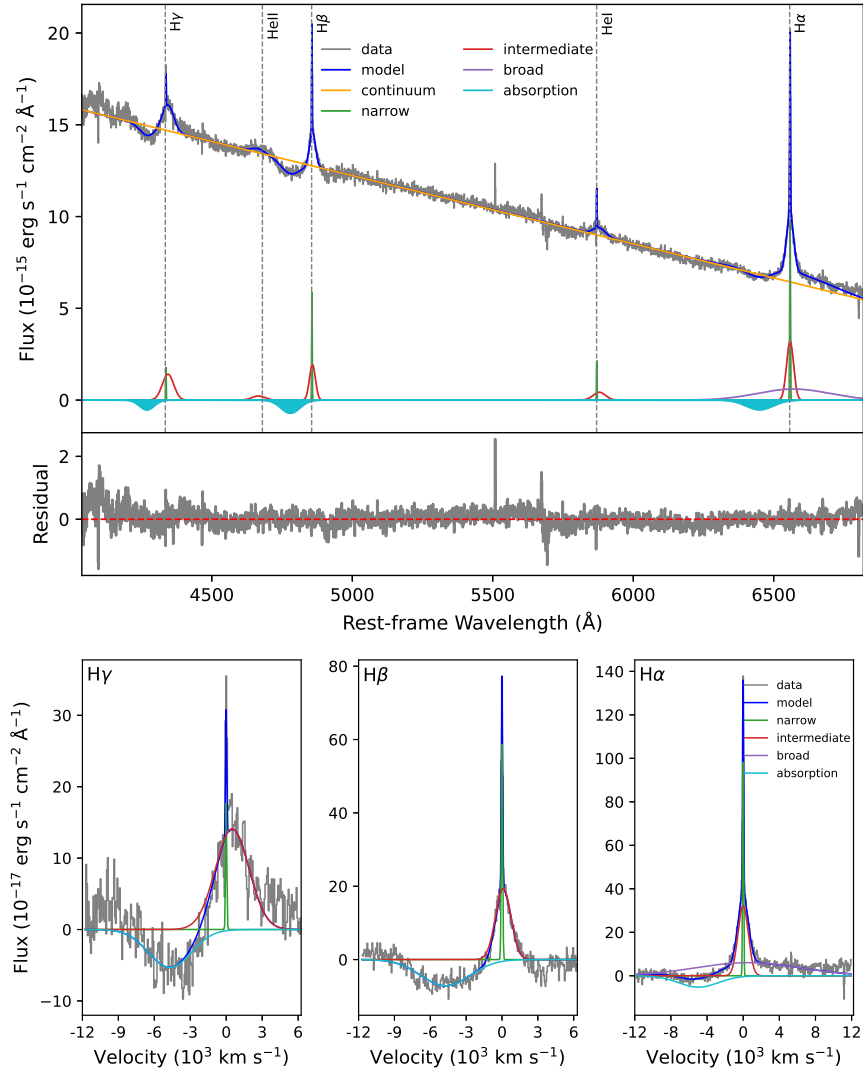
## 2 Optical spectrum analysis

SN 2017hcd was classified as an SN IIn using a spectrum taken on October 17 2017<sup>39</sup>. We obtained this single-epoch spectrum from TNS. The spectrum is characterized by a blue continuum, hydrogen-rich features, and prominent narrow Balmer emission lines. That last characteristic is what leads to the SN IIn classification<sup>51,52</sup> (see Extended Data Fig. 3). We verified this classification by using the Supernova Identification code (SNID)<sup>53</sup>, which returned SN IIn as the best match.

We further analyzed the line features by fitting the continuum with a linear line and modeling the features with multi-component Gaussian profiles; the latter consisted of narrow, intermediate, and broad components. The best-fit parameters and their uncertainties were obtained using `emcee`. The overall fit to the spectrum and the detailed fits to the Balmer lines ( $H\alpha$ ,  $H\beta$ , and  $H\gamma$ ) are presented in Extended Data Fig. 3, and the velocity and Full Width at Half Maximum (FWHM) measurements of the lines are summarized in Extended Data Table 1. The observed spectral features, namely a P-Cygni profile with multi-component emissions, are similar to those seen in other SNe IIn (e.g., refs. 54–56). Among the components, the blue-shifted absorption feature is a direct tracer of the outflowing SN-CSM shell. For SN 2017hcd, the velocities from the absorptions at the Balmer lines were all consistently found within the range of 4700–5000 km s<sup>-1</sup>, which was likely the expansion velocity of the SN-CSM shell.

Name	Absorption		Narrow	
	Velocity	FWHM	Velocity	FWHM
H $\alpha$	$-4956^{+108}_{-108}$	$5259^{+330}_{-314}$	$-8.60^{+0.70}_{-0.60}$	$133.4^{+1.9}_{-1.8}$
H $\beta$	$-4729^{+74}_{-73}$	$4933^{+157}_{-149}$	$-2.0^{+1.3}_{-1.3}$	$127.5^{+3.0}_{-2.9}$
H $\gamma$	$-4700^{+20}_{-20}$	$4265^{+172}_{-213}$	$1^{+22}_{-20}$	$117.3^{+6.1}_{-5.7}$
Name	Intermediate		Broad	
H $\alpha$	$-6.7^{+6.6}_{-6.6}$	$1342^{+24}_{-24}$	$540^{+370}_{-353}$	$13645^{+589}_{-557}$
H $\beta$	$106^{+14}_{-14}$	$1532^{+37}_{-37}$	—	—
H $\gamma$	$500^{+20}_{-20}$	$3300^{+170}_{-164}$	—	—

Extended Data Table 1: **Fitting Results for Balmer Lines.** Parameters were derived from the multi-component Gaussian fits (Extended Data Fig. 3). The reported velocities and FWHMs are in units of km s<sup>-1</sup>, and the uncertainties are 1 $\sigma$  ranges.



Extended Data Fig. 3: **Fitting analysis for the spectrum of SN 2017hcd.** *Upper panels:* the top shows the spectrum and the fit consisting of a linear line plus multi-component Gaussian functions, and the bottom displays the residuals (data minus model) of the fitting. *Lower panels:* detailed multi-component fits to the Balmer H lines ( $H\gamma$ ,  $H\beta$ , and  $H\alpha$ ), whose continuum component is subtracted.

### 3 IceCube data analysis

**IceCube data and model setup** IceCube track-like neutrino events, originating in charged-current interactions of muon (antimuon) neutrinos with nucleons, are better suited to search for neutrino emissions from point-like sources because of their good angular resolution ( $\lesssim 1^\circ$ )<sup>57</sup>. IceCube has released the all-sky track-like neutrino events from April 2008 to July 2018<sup>58</sup>, which consist of five different data acquisition periods (seasons): IC40, IC59, IC79, IC86-I and IC86-II–VII. This 10-year dataset has been widely used for searching for neutrino emissions in both time-integrated<sup>57,59–64</sup> and time-dependent<sup>65–68</sup> analysis. The time-dependent analysis should only be performed on the data of one season because different seasons have different detector configurations. We selected the data of season IC86-II–VII, which were obtained between April 2012 to July 2018, fully encompassing the optical data period of SN 2017hcd. We employed a time-dependent maximum likelihood method<sup>69</sup>, implemented in SKYLLH released by IceCube<sup>70–72</sup>, to perform the neutrino data analysis.

We assumed a power-law energy spectrum for the neutrino emission,  $\Phi_{\nu_\mu+\bar{\nu}_\mu} = \Phi_0(E_{\nu_\mu}/E_0)^{-\gamma}$ . The flux normalization  $\Phi_0$  is determined by two free parameters, the number of signal events  $n_s$  and power-law index  $\gamma$ , as well as the effective area of the IceCube detector at the declination of the source and the duration of a flare. We set up two time profiles to search for a possible neutrino clustering: a Gaussian and a box profile. The Gaussian profile  $\mathcal{T}_S$  is defined as

$$\mathcal{T}_S(t_i|T_0, \sigma_T) = \frac{1}{\sqrt{2\pi}\sigma_T} e^{-\frac{(t_i-T_0)^2}{2\sigma_T^2}}, \quad (2)$$

where  $t_i$  is the arrival time of neutrino event  $i$ , and  $T_0$  and  $\sigma_T$  are the central time and the standard deviation of this Gaussian function, respectively. The time width  $T_W$  for such a neutrino clustering is given as  $T_W = 2\sigma_T$ . The box profile is given by a uniform distribution

$$\mathcal{T}_S(t_i|T_0, T_W) = \frac{1}{T_W} \quad (T_0 - T_W/2 \leq t_i \leq T_0 + T_W/2), \quad (3)$$

where  $T_0$  and  $T_W$  are the central time and the time width of this distribution. In our search,  $T_0$  and  $\sigma_T$  (or  $T_W$ ) were also free parameters.

**Time-dependent analysis** The SKYLLH document <sup>3</sup> provides a full description about the analysis method. Here, we briefly introduce the process in our analysis.

The time-dependent likelihood function is defined as:

$$\mathcal{L}(n_s, \gamma, T_0, T_W) = \prod_i \left[ \frac{n_s}{N} S_i(\vec{x}_i, \sigma_i, E_i, t_i | \vec{x}_S, \gamma, T_0, T_W) + \left(1 - \frac{n_s}{N}\right) B_i(\delta_i, E_i, t_i) \right], \quad (4)$$

where  $N$  is the total number of events in the data sample, and  $S_i$  and  $B_i$  are the signal and background probability density functions (PDFs) for  $i$ th neutrino event respectively.

The signal PDF is divided into the spatial, energy, and time components

$$S_i(\vec{x}_i, \sigma_i, E_i, t_i | \vec{x}_S, \gamma, T_0, T_W) = \mathcal{S}_S(\vec{x}_i, \sigma_i | \vec{x}_S) \cdot \mathcal{E}_S(E_i | \delta_i, \gamma) \cdot \mathcal{T}_S(t_i | T_0, T_W), \quad (5)$$

where  $\mathcal{S}_S$  is the point-spread-function (PSF) of the detector for a given source at position  $\vec{x}_S$ , which is described by a two-dimensional Gaussian function  $\exp(-\frac{|\vec{x}_i - \vec{x}_S|^2}{2\sigma_i^2})$ , with  $\sigma_i$  being the angular reconstruction uncertainty of event  $i$  at position  $\vec{x}_i$ . The signal energy PDF  $\mathcal{E}_S$  is the probability of detecting a neutrino event with reconstructed muon energy  $E_i$  at declination  $\delta_i$  for an assumed power-law model. The signal time PDF  $\mathcal{T}_S$  describes the temporal distribution of neutrino events and was set to be one of the two time profiles defined above.

The background PDF is similarly separated as

$$B_i(\delta_i, E_i, t_i) = \mathcal{S}_B(\delta_i) \cdot \mathcal{E}_B(E_i | \delta_i) \cdot \mathcal{T}_B(t_i). \quad (6)$$

The background spatial term  $\mathcal{S}_B$  depends only on event declination  $\delta_i$ , as the background distribution is uniform in right ascension for IceCube. The background energy PDF  $\mathcal{E}_B$  describes the

---

<sup>3</sup>[https://github.com/icecube/skylh/blob/master/doc/user\\_manual.pdf](https://github.com/icecube/skylh/blob/master/doc/user_manual.pdf)

probability for a background event and is derived directly from the experimental data. The background time PDF  $\mathcal{T}_B$  is considered to be uniform, with  $\mathcal{T}_B(t_i) = \frac{1}{T_{\text{live}}}$ , where  $T_{\text{live}}$  is the total livetime of the data.

For an event, its weight is defined as the signal-over-background ratio,

$$S_i/B_i = \frac{\mathcal{S}_S(\vec{x}_i, \sigma_i | \vec{x}_S) \cdot \mathcal{E}_S(E_i | \delta_i, \gamma)}{\mathcal{S}_B(\delta_i) \cdot \mathcal{E}_B(E_i | \delta_i)}, \quad (7)$$

which is time-independent and is only a function of  $\gamma$  for a given source position. For example, the weights of the neutrino events shown in Figs. 1 & 2 were calculated by using  $\gamma = 3.5$ , the best-fit value obtained in our analysis.

In our analysis, the best-fit values were found by maximizing the log-likelihood ratio, which is defined as the test statistic (TS)

$$\text{TS} = 2 \left[ \log \frac{\mathcal{L}(n_s, \gamma, T_0, T_W)}{\mathcal{L}(n_s = 0)} - \log(\text{pf}) \right], \quad (8)$$

where  $\mathcal{L}(n_s = 0)$  represents the null (background-only) hypothesis. A penalty factor (pf),  $\log(\text{pf}) = \log\left(\frac{T_{\text{win}}}{\sqrt{2\pi}\sigma_T}\right)$  for a Gaussian profile ( $\log\left(\frac{T_{\text{win}}}{T_W}\right)$  for a box profile), is added to correct the look-elsewhere effect<sup>67,69</sup>. The *a priori* search window  $T_{\text{win}}$  was set to be 300 days, from MJD 57950 to MJD 58250.

**Expectation Maximization method for finding flares** Expectation Maximization (EM) is an unsupervised learning algorithm<sup>73</sup> that has been applied in IceCube time-dependent analysis to identify neutrino flares<sup>67,74–76</sup>. This method can largely reduce computational cost while achieving results that are consistent with those obtained through conventional brute-force methods<sup>67,76</sup>. It is particularly efficient for cases of estimating the significance of a signal when a large number of background trials are conducted. SKYLLH currently only provides the EM fitting for a Gaussian time profile. We extended the EM fitting to include a box time profile. The procedure follows that given in refs. 67, 76.

The EM algorithm iterates between two steps: the expectation (E) step and the maximization (M) step. The E step calculates the membership probability  $P_{i,\text{flare}}$  for event  $i$  to belong to the signal distribution. For a Gaussian time profile, this probability is given as

$$P_{i,\text{flare}} = \frac{n_{\text{flare}} \frac{S_i}{B_i} \mathcal{T}(t_i|T_0, \sigma_T)}{n_{\text{flare}} \frac{S_i}{B_i} \mathcal{T}(t_i|T_0, \sigma_T) + \frac{N_{\text{data}} - n_{\text{flare}}}{T_{\text{data}}}}, \quad (9)$$

where  $n_{\text{flare}}$  denotes the expected number of signal events used only within the EM framework,  $\frac{S_i}{B_i}$  is the time-independent event weight for a given spectral index  $\gamma_{\text{EM}}$  calculated from Eq. 7, and  $N_{\text{data}}$  is the number of events in an *a priori* window, whose time length is  $T_{\text{data}}$ . For the box time profile, the time PDF is replaced by  $\mathcal{T}(t_i|T_0, T_W)$ , i.e., Eq. 3. In the M step,  $T_0$  and  $\sigma_T$  (or  $T_W$ ) are updated using the membership probabilities calculated in the E step. For both time profiles,  $T_0$  is given by

$$T_0 = \frac{\sum_i P_{i,\text{flare}} t_i}{\sum_i P_{i,\text{flare}}}. \quad (10)$$

For the Gaussian profile,  $\sigma_T$  can be directly calculated as

$$\sigma_T = \sqrt{\frac{\sum_i P_{i,\text{flare}} (t_i - T_0)^2}{\sum_i P_{i,\text{flare}}}}. \quad (11)$$

For the box profile, which is a uniform distribution, the time width can be derived as

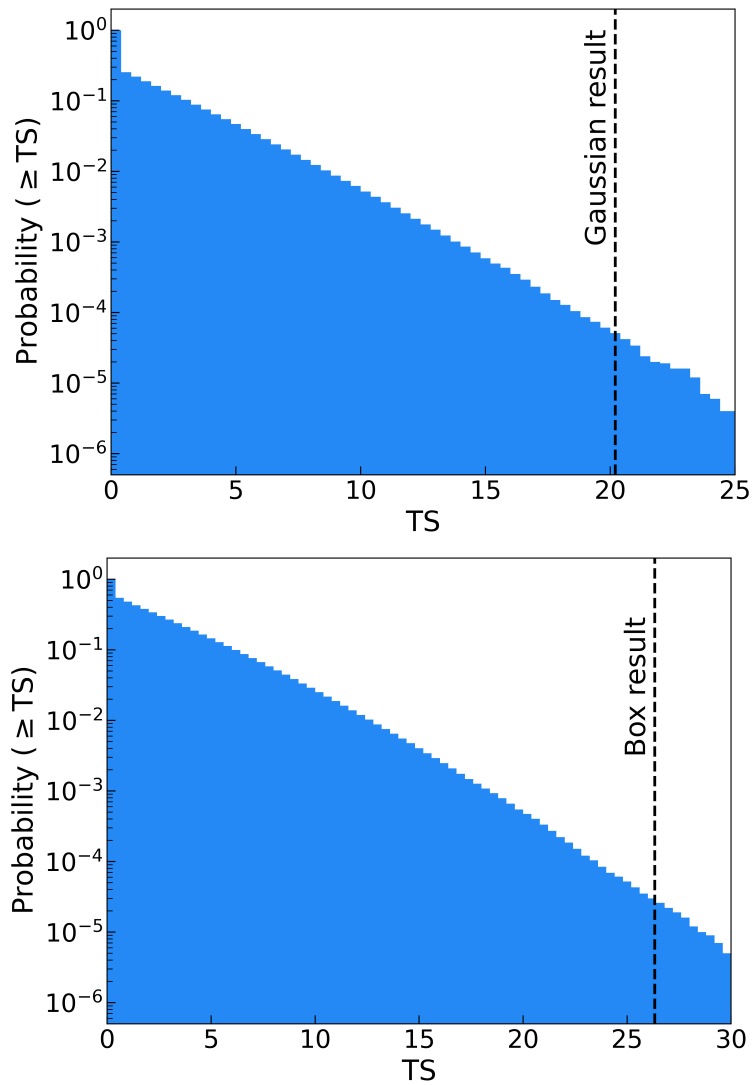
$$T_W = 2\sqrt{3} \sqrt{\frac{\sum_i P_{i,\text{flare}} (t_i - T_0)^2}{\sum_i P_{i,\text{flare}}}}. \quad (12)$$

The convergence criterion is set as either the likelihood remaining unchanged for 20 iterations or reaching a maximum number of 500 iterations<sup>67</sup>. In our analysis, EM was performed on the data within the *a priori* window to find a neutrino flare. In addition, the time width  $\sigma_T$  (or  $T_W$ ) was restricted to  $\geq 5$  days<sup>67</sup>. Upon convergence, EM returns the optimized  $T_0$  and  $\sigma_T$  (or  $T_W$ ) for a fixed  $\gamma_{\text{EM}}$ .

For the box profile, the likelihood is particularly sensitive to small variations in time due to the discontinuity of the profile. If the true signal distribution is not perfectly uniform (e.g., asymmetric),  $T_0$  and  $T_W$  derived from Eq. 10 and Eq. 12 will deviate from the actual values. Thus, we performed an additional local optimization of the box parameters in the vicinity of the optimized results given by EM. Specifically, we minimized the negative likelihood, where the EM results serve as the initial values and the bounds are set as  $T_0 \in [T_{0,EM} - T_{W,EM}/2, T_{0,EM} + T_{W,EM}/2]$  and  $T_W \in [0.5T_{W,EM}, 2T_{W,EM}]$ .

We ran the above procedures for  $\gamma_{EM}$  in the range  $[1.5, 4.0]$  <sup>76</sup> with steps of 0.1. For each  $\gamma_{EM}$ , the optimized time PDF was passed to Eq. 8 to maximize the likelihood ratio, yielding the best-fit  $n_s$  and  $\gamma$  values. The flare with the highest TS value was then identified as the best-fit flare. Overall, the parameters in the analysis were set in the ranges of  $n_s \geq 0$ ,  $\gamma \in [1.5, 4.0]$ ,  $T_0 \in [57950, 58250]$ , and  $T_W$  (or  $\sigma_T$ )  $\geq 5$  day. Because of the upper bound of 4.0 set on  $\gamma$ , the upper bound uncertainty for it was thus limited to 4.0 (Table 1).

**Detection significance estimate** We estimated the significance of the detection by performing background-only trials at the location of SN 2017hcd using randomized data. The randomized data were generated by shuffling the event times in the data sample and re-calculating the right ascension of each event. For each trial, the analysis following the same procedure as that applied to the real data was conducted. We performed  $10^6$  times background-only trials for each of the two time profiles. The resulting background TS distributions are shown in Extended Data Fig. 4. The  $p$ -value was then estimated as a fraction of any background trials that had a TS value greater than that obtained from the real-data analysis. The largest TS values we obtained were 20.2 for the Gaussian time profile and 26.3 for the box time profile, and the corresponding  $p$ -values were  $4.5 \times 10^{-5}$  ( $3.9\sigma$ ) for the former and  $2.7 \times 10^{-5}$  ( $4.0\sigma$ ) for the latter. As there was no *a priori* time profile for the flare, we considered a trial factor of 2, and the significance of the box time profile (i.e., the more significant one) was reduced to  $3.9\sigma$ .



Extended Data Fig. 4: **Background TS distributions of the Gaussian (*upper*) and box (*lower*) time profile.** The blue bar is the p-value of the background in each TS bin. The dashed lines mark the TS values obtained at the location of SN 2017hcd with the respective time profiles.

## 4 *Fermi*-LAT data analysis

We searched for possible  $\gamma$ -ray emissions from SN 2017hcd by analyzing the data obtained with the Large Area Telescope (LAT) onboard *the Fermi Gamma-ray Space Telescope (Fermi)*. We selected photon events in the energy range of 0.1–500 GeV (evclass=128 and evtype=3) from the updated *Fermi* Pass 8 database from the time range Jul. 16 2017 00:00:00 (UTC; MJD 57950) to May 12 2018 00:00:00 (UTC; MJD 58250), which was our search window  $T_{\text{win}}$  for the neutrino flare. The region of interest (RoI) was defined to be  $20^\circ \times 20^\circ$ , with the center at the position of SN 2017hcd. Events with zenith angles  $>90^\circ$  were excluded to avoid contamination from the Earth’s limb, and the expression `DATA_QUAL > 0 && LAT_CONFIG = 1` was used to obtain good time-intervals. The instrumental response function `P8R3_SOURCE_V3` and the package `Fermitools-2.2.0` were used in our analysis.

The source model was constructed from the latest (Data Release 4, DR4) *Fermi* Gamma-ray LAT (FGL) 14-year source catalog (4FGL-DR4)<sup>77</sup>. All sources in the catalog within  $25^\circ$  of the target were included, and their spectral models were adopted. In our analysis, spectral indices and normalizations of sources within  $5^\circ$  of the target were set as free parameters and all other parameters were fixed at the catalog values. The extragalactic diffuse emission and the Galactic diffuse emission components, i.e., the spectral files `iso_P8R3_SOURCE_V3_v1.txt` and `gll_iem_v07.fits`, respectively, were included as well. The normalizations of these two background components were also set as free parameters.

For possible  $\gamma$ -ray emissions from SN 2017hcd, we assumed a point source with a power-law energy spectrum,  $dN/dE_\gamma = N_0(E_\gamma/E_b)^{-\Gamma}$ , where  $E_b$  was fixed at 1 GeV. We performed the standard binned likelihood analysis<sup>4</sup> to the whole selected data in 0.1–500 GeV, and did not find significant emission at the target’s position. We also performed unbinned likelihood analysis to the data in the 54-day neutrino-emission time range (Fig. 1), and did not find significant emission

---

<sup>4</sup>[https://fermi.gsfc.nasa.gov/ssc/data/analysis/documentation/Cicerone/Cicerone\\_Likelihood/](https://fermi.gsfc.nasa.gov/ssc/data/analysis/documentation/Cicerone/Cicerone_Likelihood/)

either. Individual  $\geq 1$  GeV photons from the direction of SN 2017hcd were searched by running tool `gtsrcprob` for data within  $1^\circ$  of the SN, which is approximately the 68% containment angle of LAT's PSF at 1 GeV<sup>5</sup>. The spectral index  $\Gamma$  for an assumed source was fixed at 2. We did not find any photons with  $\geq 50\%$  probability arising from the direction of SN 2017hcd. The 95% photon-flux upper limit during the 54-day time range was estimated to be  $\sim 6 \times 10^{-9} \text{ cm}^{-2} \text{ s}^{-1}$  in the energy range of 0.1–500 GeV, which corresponds to an energy-flux upper limit of  $8.4 \times 10^{-12} \text{ erg cm}^{-2} \text{ s}^{-1}$  in the energy range of 0.1–500 GeV (where  $\Gamma = 2$  was assumed).

## References

38. Tonry, J. *et al.* ATLAS Transient Discovery Report for 2017-10-05. *Transient Name Server Discovery Report* **2017-1070**, 1 (2017).
39. Xhakaj, E. *et al.* Xhakaj, E. *et al.* Transient Classification Report for 2017-11-23. *Transient Name Server Classification Report* **2017-1308**, 1 (2017).
40. Haynes, M. P. *et al.* The Arecibo Legacy Fast ALFA Survey: The  $\alpha$ .40 H I Source Catalog, Its Characteristics and Their Impact on the Derivation of the H I Mass Function. *Astron. J.* **142**, 170 (2011). 1109.0027.
41. Shingles, L. *et al.* Release of the ATLAS Forced Photometry server for public use. *Transient Name Server AstroNote* **7**, 1–7 (2021).
42. Rest, S. *et al.* ATClean: High-Fidelity, Statistically Clean ATLAS Light Curves and Feature Detection (2023).
43. Hodgkin, S. T. *et al.* Gaia Early Data Release 3. Gaia photometric science alerts. *Astron. Astrophys.* **652**, A76 (2021). 2106.01394.
44. Chambers, K. C. *et al.* The Pan-STARRS1 Surveys. *arXiv e-prints* arXiv:1612.05560 (2016). 1612.05560.

---

<sup>5</sup>[https://www.slac.stanford.edu/exp/glast/groups/canda/lat\\_Performance.htm](https://www.slac.stanford.edu/exp/glast/groups/canda/lat_Performance.htm)

45. Chevalier, R. A. & Irwin, C. M. Shock Breakout in Dense Mass Loss: Luminous Supernovae. *Astrophys. J. Let.* **729**, L6 (2011). 1101.1111.
46. Ofek, E. O. *et al.* Interaction-powered Supernovae: Rise-time versus Peak-luminosity Correlation and the Shock-breakout Velocity. *Astrophys. J.* **788**, 154 (2014). 1404.4085.
47. Foreman-Mackey, D., Hogg, D. W., Lang, D. & Goodman, J. emcee: The MCMC Hammer. *Publ. Astron. Soc. Pac.* **125**, 306 (2013). 1202.3665.
48. Taddia, F. *et al.* Carnegie Supernova Project: Observations of Type II<sub>n</sub> supernovae. *Astron. Astrophys.* **555**, A10 (2013). 1304.3038.
49. Thornton, I., Villar, V. A., Gomez, S. & Hosseinzadeh, G. extrabol: A Python Package for Estimating Bolometric Light Curves of Thermal Transients. *Research Notes of the American Astronomical Society* **8**, 48 (2024).
50. Schlafly, E. F. & Finkbeiner, D. P. Measuring Reddening with Sloan Digital Sky Survey Stellar Spectra and Recalibrating SFD. *Astrophys. J.* **737**, 103 (2011). 1012.4804.
51. Schlegel, E. M. A new subclass of type II supernovae ? *Mon. Not. R. Astron. Soc.* **244**, 269–271 (1990).
52. Filippenko, A. V. Optical Spectra of Supernovae. *Annu. Rev. Astron. Astrophys.* **35**, 309–355 (1997).
53. Blondin, S. & Tonry, J. L. Determining the Type, Redshift, and Age of a Supernova Spectrum. *Astrophys. J.* **666**, 1024–1047 (2007). 0709.4488.
54. Terreran, G. *et al.* The Early Phases of Supernova 2020pni: Shock Ionization of the Nitrogen-enriched Circumstellar Material. *Astrophys. J.* **926**, 20 (2022). 2105.12296.

55. Hiramatsu, D. *et al.* Multiple Peaks and a Long Precursor in the Type II<sub>n</sub> Supernova 2021qqp: An Energetic Explosion in a Complex Circumstellar Environment. *Astrophys. J.* **964**, 181 (2024). 2305.11168.
56. Baer-Way, R. *et al.* A Multiwavelength Autopsy of the Interacting Type II<sub>n</sub> Supernova 2020ywx: Tracing Its Progenitor Mass-loss History for 100 Yr Before Death. *Astrophys. J.* **983**, 101 (2025). 2412.06914.
57. Aartsen, M. G. *et al.* Time-Integrated Neutrino Source Searches with 10 Years of IceCube Data. *Phys. Rev. Lett.* **124**, 051103 (2020). 1910.08488.
58. IceCube Collaboration *et al.* IceCube Data for Neutrino Point-Source Searches Years 2008-2018. *arXiv e-prints* arXiv:2101.09836 (2021). 2101.09836.
59. Zhou, B., Kamionkowski, M. & Liang, Y.-f. Search for high-energy neutrino emission from radio-bright AGN. *Phys. Rev. D* **103**, 123018 (2021). 2103.12813.
60. Abbasi, R. *et al.* Search for Astrophysical Neutrinos from 1FLE Blazars with IceCube. *Astrophys. J.* **938**, 38 (2022). 2207.04946.
61. Huang, T.-Q. & Li, Z. Neutrino observations of LHAASO sources: Present constraints and future prospects. *Mon. Not. R. Astron. Soc.* **514**, 852–862 (2022). 2112.14062.
62. Neronov, A., Savchenko, D. & Semikoz, D. V. Neutrino Signal from a Population of Seyfert Galaxies. *Phys. Rev. Lett.* **132**, 101002 (2024). 2306.09018.
63. Li, W., Huang, T.-Q., Xu, D. & He, H. Search for Neutrino Signals Correlated with LHAASO Diffuse Galactic Emission. *Astrophys. J.* **980**, 164 (2025). 2408.12123.
64. Ji, S., Wang, Z., Zheng, D. & Zheng, J. Possible Neutrino Emission from the Pulsar Wind Nebula G63.7+1.1. *Astrophys. J.* **990**, 142 (2025). 2507.19724.

65. Abbasi, R. *et al.* Search for Multi-flare Neutrino Emissions in 10 yr of IceCube Data from a Catalog of Sources. *Astrophys. J. Let.* **920**, L45 (2021). 2109.05818.
66. Lucarelli, F. *et al.* Neutrino search from  $\gamma$ -ray bursts during the prompt and X-ray afterglow phases using 10 years of IceCube public data. *Astron. Astrophys.* **672**, A102 (2023). 2208.13792.
67. Abbasi, R. *et al.* Search for Continuous and Transient Neutrino Emission Associated with IceCube’s Highest-energy Tracks: An 11 yr Analysis. *Astrophys. J.* **964**, 40 (2024). 2309.12130.
68. Li, R.-L. *et al.* A neutrino flare potentially associated with X-ray emission from tidal disruption event ATLAS17jrp. *arXiv e-prints* arXiv:2411.06440 (2024). 2411.06440.
69. Braun, J. *et al.* Time-dependent point source search methods in high energy neutrino astronomy. *Astroparticle Physics* **33**, 175–181 (2010). 0912.1572.
70. Bellenghi, C. *et al.* Extending SkyLLH software for neutrino point source analyses with 10 years of IceCube public data. *PoS ICRC2023*, 1061 (2023).
71. Abbasi, R. *et al.* The SkyLLH framework for IceCube point-source search. *PoS ICRC2021*, 1073 (2021).
72. Wolf, M. SkyLLH - A generalized Python-based tool for log-likelihood analyses in multi-messenger astronomy. *PoS ICRC2019*, 1035 (2019).
73. Dempster, A. P., Laird, N. M. & Rubin, D. B. Maximum likelihood from incomplete data via the em algorithm. *Journal of the Royal Statistical Society. Series B (Methodological)* **39**, 1–38 (1977). URL <http://www.jstor.org/stable/2984875>.
74. Karl, M. *et al.* Search for high-energy neutrino sources from the direction of IceCube alert events. In *37th International Cosmic Ray Conference*, 940 (2022). 2107.08853.

75. Karl, M. S. *Unraveling the origin of high-energy neutrino sources: follow-up searches of IceCube alert events*. Ph.D. thesis, Munich, Tech. U. (2022).
76. Karl, M. & Eller, P. Fast identification of transients: applying expectation maximization to neutrino data. *Journal of Cosmology and Astroparticle Physics* **2024**, 057 (2024). 2312.15196.
77. Ballet, J., Bruel, P., Burnett, T. H., Lott, B. & The Fermi-LAT collaboration. Fermi Large Area Telescope Fourth Source Catalog Data Release 4 (4FGL-DR4). *arXiv e-prints* arXiv:2307.12546 (2023). 2307.12546.

**Acknowledgments** This work has made use of data from the Asteroid Terrestrial-impact Last Alert System (ATLAS) project. The Asteroid Terrestrial-impact Last Alert System (ATLAS) project is primarily funded to search for near earth asteroids through NASA grants NN12AR55G, 80NSSC18K0284, and 80NSSC18K1575; byproducts of the NEO search include images and catalogs from the survey area. This work was partially funded by Kepler/K2 grant J1944/80NSSC19K0112 and HST GO-15889, and STFC grants ST/T000198/1 and ST/S006109/1. The ATLAS science products have been made possible through the contributions of the University of Hawaii Institute for Astronomy, the Queen’s University Belfast, the Space Telescope Science Institute, the South African Astronomical Observatory, and The Millennium Institute of Astrophysics (MAS), Chile.

We acknowledge ESA Gaia, DPAC and the Photometric Science Alerts Team (<http://gsaweb.ast.cam.ac.uk/alerts>).

This research is supported by the National Natural Science Foundation of China (11633007) and the Xingdian Talent Support Project of the Yunnan Province (XDYC-YLXZ-2023-0016). S.J. acknowledges the support from the Yunnan Provincial Department of Education Scientific Research Fund and the Yunnan University Graduate Student Research Program (KC-252512068).

**Author contributions** S.J. made the initial discovery, conducted the IceCube data analysis, and wrote the initial text for the Methods sections. Z.W. formed the concept for the discovery and wrote most of the text. L.Z. analyzed the optical spectrum data. D.Z. analyzed the Fermi-LAT data.

**Competing Interests** The authors declare no competing interests.

**Correspondence** Correspondence and requests for materials should be addressed to Zhongxiang Wang ([wangzx20@ynu.edu.cn](mailto:wangzx20@ynu.edu.cn)).